An estimate of equilibrium climate sensitivity from interannual variability

A.E. Dessler[1]*, P.M. Forster[2]

[1] Dept. of Atmospheric Sciences, Texas A&M University. adessler@tamu.edu

[2] School of Earth and Environment, University of Leeds, UK p.m.forster@leeds.ac.uk

Main points:

1. We use interannual variability to estimate equilibrium climate sensitivity (ECS). We estimate ECS is *likely* 2.4-4.5 K (17-83% confidence interval), with a mode and median value of 2.9 and 3.3 K, respectively.
2. We see no evidence to support low ECS (values less than 2K) suggested by recent analyses.
3. This work shows the value of alternate energy balance frameworks for understanding climate change.

Abstract

Estimating the equilibrium climate sensitivity (ECS; the equilibrium warming in response to a doubling of CO_2) from observations is one of the big problems in climate science. Using observations of interannual climate variations covering the period 2000 to 2017, we estimate ECS is *likely* 2.4-4.5 K (17-83% confidence interval), with a mode and median value of 2.9 and 3.3 K, respectively. Our analysis provides no support for low values of ECS (below 2 K) suggested by other analyses. The main uncertainty in our estimate is not observational uncertainty, but rather uncertainty in converting observations of short-term, mainly unforced climate variability to an estimate of the response of the climate system to long-term forced warming.

Plain language summary

Equilibrium climate sensitivity is the amount of warming resulting from doubling carbon dioxide. It is one of the important metrics in climate science because it is a primary determinant of how much warming we will experience in the future. Despite decades of work, this quantity remains uncertain: the last IPCC report stated a range for ECS of 1.5-4.5 deg. Celsius. Using observations of interannual climate variations covering the period 2000 to 2017, we estimate ECS is *likely* 2.4-4.5 K. Thus, our analysis provides no support for the bottom of the IPCC's range.

Introduction

The response of the climate system to the imposition of a climate forcing is frequently expressed using the linearized energy balance equation:

$$R = F + \lambda T_s \quad (1)$$

where forcing F is an imposed top-of-atmosphere (TOA) energy imbalance, T_S is the global average surface temperature, and λ is the change in TOA flux per unit change in T_S [Sherwood *et al.*, 2014]. R is the resulting TOA flux imbalance from the combined forcing and response. All quantities are deviations from an equilibrium base state, usually the pre-industrial climate. Equilibrium climate sensitivity (hereafter ECS, the equilibrium warming in response to a doubling of CO_2) can be calculated as:

$$ECS = -F_{2xCO2}/\lambda \quad (2)$$

where F_{2xCO2} is the forcing from doubled CO_2.

Equation 1 is a workhorse of climate science and it has been used many times to estimate λ and ECS. Many of these [e.g., Gregory *et al.*, 2002; Annan and Hargreaves, 2006; Otto *et al.*, 2013; Lewis and Curry, 2015; Aldrin *et al.*, 2012; Skeie *et al.*, 2014; Forster, 2016] combine Eq. 1 with estimates of R, F, and T_s over the 19th and 20th centuries to infer λ and ECS. These calculations suggest λ is near -2 W/m^2/K and appear to rule out an ECS larger than ~4 K [Stevens *et al.*, 2016]. The increased likelihood of an ECS below 2 K implied by these calculations led the IPCC Fifth Assessment Report (AR5) to extend their *likely* ECS range downward to include 1.5 K [Collins *et al.*, 2013].

However, since AR5 a number of problems with this approach have been identified. These include questions about the impact of internal variability [e.g., Dessler *et al.*, 2018], arguments that ECS inferred from historical energy budget produces an underestimate of the true value [e.g., Armour, 2017; Gregory and Andrews, 2016; Zhou *et al.*, 2016; Andrews and Webb, 2018; Proistosescu and Huybers, 2017; Marvel *et al.*, 2018], the large and evolving uncertainty in forcing over the 20th century [e.g., Forster, 2016], different forcing efficacies of greenhouse

gases and aerosols [Shindell, 2014; Kummer and Dessler, 2014], and geographically incomplete or inhomogeneous observations [Richardson *et al.*, 2016].

For robust estimates of ECS, multiple lines of evidence are needed and care needs to be taken in relating the inferred ECS from any method to other estimates. Thus, there is great value in finding alternate ways to approach the problem. Relatively few papers have attempted use short-term interannual variability to estimate ECS [e.g., Forster, 2016; Tsushima *et al.*, 2005; Forster and Gregory, 2006; Chung *et al.*, 2010; Tsushima and Manabe, 2013; Dessler, 2013; Donohoe *et al.*, 2014]. Papers that do typically yield estimates of ECS consistent with the IPCC's canonical ECS range of 1.5-4.5°C, but their uncertainty is so large as to provide no meaningful constraint of the range. In this paper, we present a new methodology to infer ECS from these interannual fluctuations of the climate system.

Results

Traditional energy-balance framework

Per Eq. 2, ECS requires estimates of $-F_{2xCO2}$ and λ. We obtain an estimate of F_{2xCO2} from fixed sea surface temperature and sea-ice experiments from ten global climate models that submitted output to the Precipitation Driver Response Model Intercomparison Project [Myhre *et al.*, 2017b]. They estimate F_{2xCO2} to be normally distributed with a mean of 3.69 W/m^2 and a standard deviation of 0.13 W/m^2.

An estimate of λ can be obtained from observations of R and T_S. Observations of R come from the Clouds and the Earth's Radiant Energy System (CERES) Energy Balanced and Filled product (ed. 4) [Loeb *et al.*, 2018] and cover the period March 2000 to July 2017. Estimates of T_S come from the European Centre for Medium Range Weather Forecasts (ECMWF) Interim Re-Analysis (ERAi) [Dee *et al.*, 2011]. Given these data, we calculate λ two ways, both based on Eq. 1. First, we assume forcing changes linearly over this time period and account for it by detrending R and T_S time series; λ is then the slope of the regression of these detrended time series. Second, we use estimates of forcing F over the CERES period and calculate λ as the slope of the regression of R-F vs. T_S. See the appendix for more details about this calculation.

Distributions of λ for the two approaches (estimated by Monte Carlo methods) are both quite wide (Fig. 1), with 5-95% confidence intervals of -1.45 to -0.15 W/m^2/K and -1.08 to +0.09 W/m^2/K for the detrended and R-F calculations, respectively. This is a consequence of the weak control T_S exerts on R in the observations [Xie *et al.*, 2016; Dessler *et al.*, 2018], and it means that our observational estimate of λ is quite uncertain. The medians of the two distributions are -0.81 and -0.50 W/m^2/K, respectively.

The distributions of λ plotted in Fig. 1 are derived mainly from the response to interannual variability, so we will refer to them hereafter as λ_{iv}. The λ in Eq. 2, however, is the climate system's response to forcing from doubled CO_2 (hereafter λ_{2xCO2}), so we cannot simply plug λ_{iv} into Eq. 2 to derive ECS. In fact, this disconnect between what we can measure (λ_{iv}) and what is required to calculate ECS (λ_{2xCO2}) is one reason scientists have largely avoided using interannual variability to infer ECS.

We therefore modify Eq. 2 to account for this:

$$\mathrm{ECS} = -\frac{F_{2\times CO2}}{\lambda_{iv}}\frac{\lambda_{iv}}{\lambda_{2\times CO2}} \qquad (3)$$

where the ratio $\lambda_{iv}/\lambda_{2xCO2}$ is a transfer function that converts the measured λ_{iv} into the required value λ_{2xCO2}. In our ECS calculations, we estimate this transfer function using models that submitted required output to the 5th phase of the Coupled Model Intercomparison Project (CMIP5) [Taylor *et al.*, 2012]. The numerator λ_{iv} is derived from the models' control runs, in which climate variations arise naturally from internal variability. The denominator is derived from a forced run of the same model.

The CMIP5 archive does not include appropriate doubled CO_2 runs, but it does have abrupt 4xCO_2 runs from which we can estimate λ_{4xCO2}. Given that, we'll assume that $\lambda_{2xCO2} \approx \lambda_{4xCO2}$, so we can re-write Eq. 3 as:

$$\mathrm{ECS} \approx -\frac{F_{2\times CO2}}{\lambda_{iv}}\frac{\lambda_{iv}}{\lambda_{4\times CO2}} \qquad (4)$$

Recent work suggests that λ_{2xCO2} is more negative (i.e., implying a lower ECS) than λ_{4xCO2} [Armour, 2017; Proistosescu and Huybers, 2017]. On the other hand, we use all 150 years of the $4xCO_2$ runs to estimate λ_{4xCO2}, which also tends to produce values that are too negative [Andrews *et al.*, 2015; Rugenstein *et al.*, 2016; Rose and Rayborn, 2016; Armour, 2017]. These two errors tend to cancel, but how much of a bias is left — and in which direction — remains an uncertainty in this analysis. The CMIP5 ensemble distribution of $\lambda_{iv}/\lambda_{4xCO2}$ is plotted in Fig. 2; it has an average of 0.81 and a standard deviation of 0.34. See the appendix for details of the calculations.

We then use a Monte Carlo approach to estimate ECS. We produce 500,000 estimates of ECS by randomly sampling the distributions of F_{2xCO2}, λ_{iv} (Fig. 1), and $\lambda_{iv}/\lambda_{4xCO2}$ (Fig. 2) and plugging them into Eq. 3; negative ECS values or values greater than 10 K are viewed as implausible and thrown out. We produce two ECS distributions — one using λ_{iv} from the detrended calculation and one using λ_{iv} from the R-F calculation.

The ECS distributions (Fig. 3) have 17-83% confidence intervals (corresponding to the IPCC's *likely* range) of 2.0-5.7 K and 2.6-7.1 K for the detrended and R-F calculations, respectively. The modes are 2.4 and 3.3 K, while the medians are 3.2 and 4.4 K. Overall, our calculated ECS distributions overlap substantially with the IPCC's range, although our distributions are shifted to higher values: we see a 29% chance that ECS exceeds 4.5 K, while the IPCC assigns that a 17% chance. Perhaps more importantly, we see less support for low values of ECS: the chance of an ECS below 2 K is 11%, while the IPCC assigns a 17% chance it is below 1.5 K. See tables in the appendix for other relevant metrics of the distributions.

Modified energy-balance framework

Recently, Dessler et al. [2018] suggested a revision of Eq. 1, where the TOA flux is parameterized in terms of tropical atmospheric temperature, not global surface temperature:

$$R = F + \Theta T_A \qquad (5)$$

where T_A is the tropical average (30°N-30°S) 500-hPa temperature and Θ converts this quantity to TOA flux. R and F are the same global average quantities they were in equation 1. They demonstrated that this way of describing energy balance has advantages over the conventional approach described in Eq. 1.

In this framework, the equilibrium warming of the tropical atmosphere ΔT_A is equal to $-F_{2xCO2}/\Theta$. ECS can therefore be written:

$$\mathrm{ECS} = -\frac{F_{2\times CO2}}{\Theta_{iv}}\frac{\Theta_{iv}}{\Theta_{2\times CO2}}\frac{\Delta T_S}{\Delta T_A} \approx -\frac{F_{2\times CO2}}{\Theta_{iv}}\frac{\Theta_{iv}}{\Theta_{4\times CO2}}\frac{\Delta T_S}{\Delta T_A} \quad (6)$$

where Θ_{iv} is the analog to λ_{iv}, $\Theta_{iv}/\Theta_{2xCO2}$ is the transfer function that allows us to use short-term variability to estimate ECS, and $\Delta T_S/\Delta T_A$ is the ratio of the temperature changes at equilibrium. As we did above, we will further assume that $\Theta_{4xCO2} \approx \Theta_{2xCO2}$.

We use the same forcing F_{2xCO2} that was used in the previous section. The distributions of the scaling factor $\Theta_{iv}/\Theta_{4xCO2}$ (Fig. 4a) and temperature ratio $\Delta T_S/\Delta T_A$ (Fig. 5a) both come from the CMIP5 ensemble (see appendix for more details), with ensemble averages and standard deviations of 0.99±0.40 and 0.86±0.10, respectively.

Just as we did for λ_{iv}, we calculate Θ_{iv} from observations two ways: by regressing detrended R vs. detrended T_A and by regressing R-F vs. T_A. The 5-95% confidence intervals are -1.37 to -0.80 W/m^2/K and -1.26 to -0.69 W/m^2/K, respectively. The means of the two distributions are also similar, with values of -1.09 and -0.98 W/m^2/K. Because of their similarities, in the rest of this section we will show results using the detrended Θ_{iv} calculation, although results for both distributions can be found in tables in the appendix.

As in the previous section, we use a Monte Carlo approach and produce 500,000 estimates of ECS by randomly sampling the distributions of F_{2xCO2}, Θ_{iv}, $\Theta_{iv}/\Theta_{4xCO2}$, and $\Delta T_S/\Delta T_A$, and then plugging the values into Eq. 6. The resulting ECS distribution (Fig. 6a) shows a similar structure to the λ-based distributions in Fig. 3: a broad maximum between 2 and 3 K and a tail towards higher ECS values.

166 There is also a puzzling peak below 1°C. The only way for an ECS estimate to be close to zero is
167 if Θ_{iv} is very large or one of the other terms in Eq. 6 is close to zero. Analysis of the terms in Eq.
168 6 suggests that the term causing the low ECS values is $\Theta_{iv}/\Theta_{4xCO2}$, whose distribution
169 approaches zero (Fig. 4a). These low values come from the GISS models (Fig. 7a) and if they are
170 removed from the ensemble, the bump below 1 K disappears (Fig. 6b), although the statistics of
171 the distribution do not change much.

172 This result emphasizes that the scaling factor $\Theta_{iv}/\Theta_{4xCO2}$ is unconstrained by observations. That
173 doesn't mean, however, that we know nothing about it — we do have observations of Θ_{iv} and
174 can compare those to each model's value of Θ_{iv}. We find that 15 of the 25 CMIP5 models
175 produce estimates of Θ_{iv} in agreement with the CERES observations (Fig. 7b). If we limit the
176 distributions of $\Theta_{iv}/\Theta_{4xCO2}$ and $\Delta T_S/\Delta T_A$ to just those models (Figs. 4b and 5b), we obtain the ECS
177 distribution in Fig. 6c (hereafter referred to as the "good-Θ" distribution).

178 We consider the "good-Θ" ECS distributions to be the best estimates of ECS from this analysis.
179 Those ECS distributions have 17-83% confidence intervals (corresponding to the IPCC's *likely*
180 range) of 2.4-4.4 K and 2.4-4.7 K for the detrended and R-F calculations, respectively. Averaging
181 these gives us our single best estimate for the *likely* range, 2.4-4.5 K, and 5-95% range, 2.0-5.6
182 K. The modes are 3.1 and 2.6 K (average 2.9 K), and the medians of both are 3.3 K.

183 These distributions suggest a 15-20% chance ECS exceeds 4.5 K and a 5% chance of an ECS
184 below 2 K. We therefore conclude that the IPCC's upper end of the *likely* ECS range is about
185 right, but that the low end is too low. We would conclude that, in the parlance of the IPCC, ECS
186 is *very unlikely* to be below 2 K.

187 **Discussion**

188 There are several reasons why ECS estimated from the revised energy balance framework (Eq.
189 6) should be considered more reliable than that estimated from the traditional framework (Eq.
190 4). Fig. 1 shows the main advantage — that Θ_{iv} is better constrained by observations than λ_{iv}.
191 This is what leads to the narrower distributions of ECS in Fig. 6 than in Fig. 3. One particular

facet of the λ_{iv} distributions is that they have non-zero probabilities of λ_{iv} values close to zero; since ECS goes as $1/\lambda_{iv}$, this leads to the generation of a large tail towards unrealistically large values.

There are additional reasons that lead us to conclude that the estimates from the revised framework are superior. It has been suggested that λ_{iv} exhibits significant decadal variability in models [Andrews *et al.*, 2015; Gregory and Andrews, 2016; Zhou *et al.*, 2016; Dessler *et al.*, 2018]. This opens the possibility that the observed λ_{iv}, which is based on 16 years of data, is biased with respect to the long-term average; if so, then ECS estimated from these observations would also be biased. Model simulations suggest that Θ_{iv} exhibits smaller decadal variability [Dessler *et al.*, 2018], making Θ_{iv} estimated from CERES data a more robust estimate of the climate system's actual long-term value. There is also evidence that Θ changes less than λ during transient climate change [Dessler *et al.*, 2018], meaning the assumption that $\Theta_{2xCO2} \approx \Theta_{4xCO2}$ is a far better assumption than the assumption that $\lambda_{4xCO2} \approx \lambda_{2xCO2}$.

It is also worth stepping back and asking what could cause our calculation to be seriously in error. It seems unlikely that forcing from doubled CO_2 is wrong given our good understanding of the physics of CO_2 forcing [e.g., Feldman *et al.*, 2015]. Estimates of λ_{iv} and Θ_{iv} are derived from observations we view to be reliable, so our judgment is that they are also unlikely to be significantly wrong. The $\Delta T_S/\Delta T_A$ term comes from climate model simulations, but models have long been able to accurately reproduce the observed pattern of warming [e.g., Stouffer and Manabe, 2017], and we have data that can be used to validate this ratio (see appendix).

Thus, the transfer function $\Theta_{iv}/\Theta_{4xCO2}$ seems the most probable place for a significant error to occur. The ratio's distribution (Fig. 4) comes from climate model simulations; we have no way to observationally validate it, nor any theory to guide us. However, as discussed previously, we can compare observations of the numerator, Θ_{iv}, to the models, and find that the majority of models produce values that agree with observations (Fig. 7). Thus, a large error in $\Theta_{iv}/\Theta_{4xCO2}$ would require a large error in Θ_{4xCO2} that does not similarly influence Θ_{iv}. While that cannot be ruled out, we see no reason to believe such an error exists.

We can also gain insight into this question by constructing an error budget to determine which term contributes most to the width of the distributions in Fig. 6. We do this by sequentially setting each term to have zero uncertainty by replacing that term's distribution in the Monte Carlo calculation with a single number, the ensemble average. This has little effect on the mean, median, or mode, but does change the width of the distribution. By comparing the widths of the resulting distributions (defined as the distance between the 17th and 83rd percentiles), we find that the biggest contributor to ECS uncertainty is the uncertainty in the $\Theta_{iv}/\Theta_{4xCO2}$ (Fig. 8). Eliminating the uncertainty on that reduces the 17-83% confidence interval to 2.8-4.0 K. *Thus, developing a theoretical argument for the value of this ratio would be a key advance in climate science.* The next most important uncertainty is the uncertainty in Θ_{iv}, followed by the uncertainty in $\Delta T_S/\Delta T_A$ and then the uncertainty in F_{2xCO2}.

Conclusions

Estimating ECS from observations remains one of the big problems in climate science. Despite several decades of intense investigations, the uncertainty in this parameter remains stubbornly large, with the last IPCC assessment reporting a *likely* range of 1.5-4.5 K (17-83% confidence interval). Because of this, there is great value in finding alternate ways to approach the problem.

In this paper, we have used observations of interannual climate variations covering the period 2000 to 2017 to estimate ECS. We interpret the observations using a modified energy balance framework (Eq. 5) in which the response of TOA flux is proportional to the atmospheric temperature.

We conclude ECS is *likely* 2.4-4.5 K (17-83% confidence interval), with a mode and median value of 2.9 and 3.3 K, respectively. Overall, our analysis suggests that the upper end of the IPCC's range is set about right, but we see little evidence to support estimates of ECS in the bottom third of the IPCC's *likely* range.

One of the key parts of our calculations is the use of CMIP5 climate models to convert the observations of interannual variability into an estimate of the response of the system to

doubled CO_2. This is the main uncertainty in our analysis and future efforts to pin this transfer function down would be extremely valuable.

Appendix

λ_{4xCO2} and Θ_{4xCO2} are calculated from CMIP5 abrupt $4xCO_2$ runs using the Gregory method [Gregory *et al.*, 2004]. In these calculations, we regress all 150 years of annual R vs. annual average temperature, and the resulting slope is λ_{4xCO2} or Θ_{4xCO2}, depending on which temperature is used (T_S for λ and T_A for Θ). Table 1 lists values for each model.

λ_{iv} and Θ_{iv} are calculated from the CMIP5 control runs. To facilitate comparison with the observations, as well as avoid any issues with long-term drift in the control runs, we break each control run into 16-year segments and calculate monthly anomalies of ΔR, ΔT_S, ΔT_A during each segment (anomalies are departures from the mean annual cycle). Then, we calculate λ_{iv} and Θ_{iv} for each segment as the slope of the regression of ΔR vs. ΔT_S or ΔT_A for that segment. We average the segments' values to come up with a single value for each model. Table 1 lists values for each model.

Observational estimates of λ_{iv} and Θ_{iv} come from measurements of R from the CERES Energy Balanced and Filled product (ed. 4) [Loeb *et al.*, 2018] and cover the period March 2000 to July 2017. The CERES time series is stable to better than 0.5 W/m^2/decade (stability of the shortwave is 0.3 W/m^2/decade [Loeb *et al.*, 2007], and longwave is 0.15 W/m^2/decade [Susskind *et al.*, 2012]). Our sign convention throughout the paper is that downward fluxes are positive, which means λ and Θ must be negative for a stable climate.

In the detrended calculations, the time series are detrended by subtracting off the linear trend estimated using an ordinary linear least-squares regression. In the R-F calculations, we use radiative forcing estimates based on IPCC AR5 [Myhre *et al.*, 2013], updated to July 2017 using greenhouse gas data from NOAA and ECLIPSE (Evaluating the Climate and Air Quality Impacts of Short-Lived Pollutants) [Hofmann *et al.*, 2006; Stohl *et al.*, 2015]. These data include a higher methane forcing estimate [Etminan *et al.*, 2016], and updated ozone and anthropogenic aerosol forcing data [Myhre *et al.*, 2017a]. The time-series of solar irradiance data is extended using

data from the Solar Radiation and Climate Experiment (SORCE) experiment [Lean *et al.*, 2005] and volcanic forcing data from NASA/GISS (https://data.giss.nasa.gov/modelforce/strataer/) with a revised relationship of 17 Wm^{-2} per unit optical depth of stratospheric aerosol [Gregory *et al.*, 2016]. Uncertainty is estimated using IPCC AR5 radiative forcing uncertainties from 2015. We take the 5%-95% range for each of the 14 different forcing terms in 2015 and turn this into a fractional range by dividing by the median 1750-2015 forcing estimate. This fractional uncertainty is Monte Carlo sampled 100,000 times for each forcing term independently. These fractions are then multiplied by the relevant forcing time series and summed to create 100,000 different realizations of the time series of total radiative forcing.

The distributions of λ_{iv} and Θ_{iv} in Fig. 1 are estimated by randomly sampling (with replacement) the detrended R or R-F and temperature time series. Each resampled data set is regressed and the slope provides one estimate λ_{iv} or Θ_{iv}. We adjust for autocorrelation of the time series by reducing the number of samples taken following Santer et al. [2000].

To evaluate the accuracy of the CMIP5 ensemble's estimate of $\Delta T_S/\Delta T_A$, we re-write it as the product of two terms:

$$\frac{\Delta T_S}{\Delta T_A} = \frac{\Delta T_{S,tropics}}{\Delta T_A} \frac{\Delta T_S}{\Delta T_{S,tropics}} \quad (7)$$

where $\Delta T_{S,tropics}$ is the tropical (30°N-30°S) average surface temperature change. The term $\Delta T_{S,tropics}/\Delta T_A$ is a measure of the tropical lapse rate, which is understood to be controlled by moist convective adjustment [Xu and Emanuel, 1989]. Fig. 9a plots monthly average anomalies of $\Delta T_{S,tropics}$ vs. ΔT_A from the ERAi and, as expected, there is a clear correlation between these variables. The slope derived from this regression is 0.51±0.06 (5-95% confidence interval).

The ERAi data set, covering 1979-2016 (37 years), contains both long-term warming and interannual variability. Because of this, we compare the ERAi results to what we consider to be the most analogous model period, the last 37 years of the CMIP5 ensemble's 150-year abrupt $4xCO_2$ runs. Ensemble average $\Delta T_{S,tropics}$ over this period is 1.07 K, similar to the warming in the

298 ERAi from 1979-2016. While a few models appear to have issues with this metric, there is
299 generally good agreement between the models and from observations (Fig. 9b).

300 The second term on the right-hand side, $\Delta T_S/\Delta T_{S,tropics}$, is a measure of polar amplification in the
301 pattern of surface warming. We estimate this by differencing the averages of the first and last
302 decade of observations or models. The ECMWF 20th century reanalysis [Poli *et al.*, 2016]
303 produces a value of 1.20 over the years 1900-2010 while the NOAA 20th century reanalysis
304 project [Compo *et al.*, 2011] produces a value of 1.23 over the years 1851-2014. We estimate
305 this ratio in each CMIP5 abrupt 4xCO_2 run and the ensemble agrees well with observations (Fig.
306 11), with a CMIP5 ensemble average of 1.18 and standard deviation of 0.11. Such good
307 agreement is not surprising — climate models have long demonstrated considerable skill in
308 simulating the large-scale patterns of surface warming [e.g., Stouffer and Manabe, 2017].

309 Tables 2, 3, and 4 contain the numerical results from the ECS distributions using λ (Eq. 4), Θ (Eq.
310 6), and the error budget, respectively. The tables include the average, mode, median, 17-83%
311 range, 5-95% range, and the probability of an ECS below 2 K or above 4.5 K.

312 The names contain "all" or "good" depending on whether they include all models or just the
313 ones whose λ_{iv} or Θ_{iv} agree with the observations. The names also include "-1" or "-2". The
314 "-1" results use λ_{iv} or Θ_{iv} derived using estimates of forcing (the R-F calculations) while the "-2"
315 use estimates from the detrended calculations.

316 In Table 3, the "noGiss" results include all models other than the two GISS models. In the
317 "good-Theta-1-corr" result, each Monte Carlo value of ECS uses values of $\Delta T_S/\Delta T_A$ and
318 $\Theta_{iv}/\Theta_{4xCO2}$ from the same model. The results are similar to other results, showing that
319 correlation in parameters between the models has little impact on our results. In the "good-
320 Theta-1-normal" result, we replace the distributions of $\Delta T_S/\Delta T_A$ and $\Theta_{iv}/\Theta_{4xCO2}$ with normal
321 distributions having the same mean and standard deviation. This has little effect on the
322 resulting ECS distribution (compared to "good-Theta-1").

Table 4 lists the results from the error analysis calculations. For these values, we take the "good-Theta-2" calculation and sequentially set the uncertainty in one term to zero. The "-noF", "-noRat", "-nodtdt", and "-noTheta" correspond to no uncertainty in F_{2xCO2}, $\Theta_{iv}/\Theta_{4xCO2}$, $\Delta T_S/\Delta T_A$, and Θ_{iv}, respectively.

References

Aldrin, M., M. Holden, P. Guttorp, R. B. Skeie, G. Myhre, and T. K. Berntsen (2012), Bayesian estimation of climate sensitivity based on a simple climate model fitted to observations of hemispheric temperatures and global ocean heat content, Environmetrics, 23(3), 253-271, doi: 10.1002/env.2140.

Andrews, T., and M. J. Webb (2018), The Dependence of Global Cloud and Lapse Rate Feedbacks on the Spatial Structure of Tropical Pacific Warming, J. Climate, 31(2), 641-654, doi: 10.1175/jcli-d-17-0087.1.

Andrews, T., J. M. Gregory, and M. J. Webb (2015), The dependence of radiative forcing and feedback on evolving patterns of surface temperature change in climate models, J. Climate, 28(4), 1630-1648, doi: 10.1175/JCLI-D-14-00545.1.

Annan, J. D., and J. C. Hargreaves (2006), Using multiple observationally-based constraints to estimate climate sensitivity, Geophys. Res. Lett., 33(6), doi: 10.1029/2005gl025259.

Armour, K. C. (2017), Energy budget constraints on climate sensitivity in light of inconstant climate feedbacks, Nature Clim. Change, 7(5), 331-335, doi: 10.1038/nclimate3278.

Chung, E. S., B. J. Soden, and B. J. Sohn (2010), Revisiting the determination of climate sensitivity from relationships between surface temperature and radiative fluxes, Geophys. Res. Lett., 37, doi: 10.1029/2010gl043051.

Collins, M., et al. (2013), Long-term climate change: Projections, commitments and irreversibility, in Climate Change 2013: The Physical Science Basis. Contribution of Working Group I to the Fifth Assessment Report of the Intergovernmental Panel on Climate Change, edited by T. F. Stocker, D. Qin, G.-K. Plattner, M. Tignor, S. K. Allen, J. Boschung, A. Nauels, Y. Xia, V. Bex and P. M. Midgley, Cambridge University Press, Cambridge, United Kingdom and New York, NY, USA.

Compo, G. P., et al. (2011), The Twentieth Century Reanalysis Project, Q. J. R. Meteor. Soc., 137(654), 1-28, doi: 10.1002/qj.776.

354 Dee, D. P., et al. (2011), The ERA-Interim reanalysis: Configuration and performance of the data
355 assimilation system, Q. J. R. Meteor. Soc., 137(656), 553-597, doi: 10.1002/qj.828.
356 Dessler, A. E. (2013), Observations of climate feedbacks over 2000-10 and comparisons to
357 climate models, J. Climate, 26(1), 333-342, doi: 10.1175/jcli-d-11-00640.1.
358 Dessler, A. E., T. Mauritsen, and B. Stevens (2018), The influence of internal variability on
359 Earth's energy balance framework and implications for estimating climate sensitivity, Atmos.
360 Chem. Phys. Discuss., 2018, 1-21, doi: 10.5194/acp-2017-1236.
361 Donohoe, A., K. C. Armour, A. G. Pendergrass, and D. S. Battisti (2014), Shortwave and
362 longwave radiative contributions to global warming under increasing CO2, Proc. Natl. Acad.
363 Sci., 111(47), 16700-16705, doi: 10.1073/pnas.1412190111.
364 Etminan, M., G. Myhre, E. J. Highwood, and K. P. Shine (2016), Radiative forcing of carbon
365 dioxide, methane, and nitrous oxide: A significant revision of the methane radiative forcing,
366 Geophys. Res. Lett., 43(24), 12,614-612,623, doi: 10.1002/2016GL071930.
367 Feldman, D. R., W. D. Collins, P. J. Gero, M. S. Torn, E. J. Mlawer, and T. R. Shippert (2015),
368 Observational determination of surface radiative forcing by CO2 from 2000 to 2010, Nature,
369 519, 339, doi: 10.1038/nature14240.
370 Forster, P. M. (2016), Inference of climate sensitivity from analysis of Earth's energy budget,
371 Annual Review of Earth and Planetary Sciences, 44, 85-106, doi: 10.1146/annurev-earth-
372 060614-105156.
373 Forster, P. M. D., and J. M. Gregory (2006), The climate sensitivity and its components
374 diagnosed from Earth Radiation Budget data, J. Climate, 19(1), 39-52.
375 Gregory, J. M., and T. Andrews (2016), Variation in climate sensitivity and feedback parameters
376 during the historical period, Geophys. Res. Lett., 43(8), 3911-3920, doi:
377 10.1002/2016GL068406.
378 Gregory, J. M., R. J. Stouffer, S. C. B. Raper, P. A. Stott, and N. A. Rayner (2002), An
379 observationally based estimate of the climate sensitivity, J. Climate, 15(22), 3117-3121, doi:
380 10.1175/1520-0442(2002)015<3117:aobeot>2.0.co;2.
381 Gregory, J. M., T. Andrews, P. Good, T. Mauritsen, and P. M. Forster (2016), Small global-mean
382 cooling due to volcanic radiative forcing, Climate Dynamics, 47(12), 3979-3991, doi:
383 10.1007/s00382-016-3055-1.

384 Gregory, J. M., W. J. Ingram, M. A. Palmer, G. S. Jones, P. A. Stott, R. B. Thorpe, J. A. Lowe,
385 T. C. Johns, and K. D. Williams (2004), A new method for diagnosing radiative forcing and
386 climate sensitivity, Geophys. Res. Lett., 31(3), doi: 10.1029/2003gl018747.
387 Hofmann, D. J., J. H. Butler, E. J. Dlugokencky, J. W. Elkins, K. Masarie, S. A. Montzka, and P.
388 Tans (2006), The role of carbon dioxide in climate forcing from 1979 to 2004: introduction
389 of the Annual Greenhouse Gas Index, Tellus B, 58(5), 614-619, doi: 10.1111/j.1600-
390 0889.2006.00201.x.
391 Kummer, J. R., and A. E. Dessler (2014), The impact of forcing efficacy on the equilibrium
392 climate sensitivity, Geophys. Res. Lett., 41(10), 3565-3568, doi: 10.1002/2014gl060046.
393 Lean, J., G. Rottman, J. Harder, and G. Kopp (2005), SORCE contributions to new
394 understanding of global change and solar variability, Solar Physics, 230(1-2), 27-53, doi:
395 10.1007/s11207-005-1527-2.
396 Lewis, N., and J. A. Curry (2015), The implications for climate sensitivity of AR5 forcing and
397 heat uptake estimates, Climate Dynamics, 45(3), 1009-1023, doi: 10.1007/s00382-014-2342-
398 y.
399 Loeb, N. G., S. Kato, K. Loukachine, N. Manalo-Smith, and D. R. Doelling (2007), Angular
400 distribution models for top-of-atmosphere radiative flux estimation from the Clouds and the
401 Earth's Radiant Energy System instrument on the Terra satellite. Part II: Validation, Journal
402 of Atmospheric and Oceanic Technology, 24(4), 564-584.
403 Loeb, N. G., D. R. Doelling, H. Wang, W. Su, C. Nguyen, J. G. Corbett, L. Liang, C. Mitrescu,
404 F. G. Rose, and S. Kato (2018), Clouds and the Earth’s Radiant Energy System (CERES)
405 Energy Balanced and Filled (EBAF) Top-of-Atmosphere (TOA) Edition-4.0 Data Product, J.
406 Climate, 31(2), 895-918, doi: 10.1175/jcli-d-17-0208.1.
407 Marvel, K., R. Pincus, G. A. Schmidt, and R. L. Miller (2018), Internal variability and
408 disequilibrium confound estimates of climate sensitivity from observations, Geophys. Res.
409 Lett., doi: 10.1002/2017GL076468.
410 Myhre, G., et al. (2013), Anthropogenic and Natural Radiative Forcing, in Climate Change 2013:
411 The Physical Science Basis. Contribution of Working Group I to the Fifth Assessment Report
412 of the Intergovernmental Panel on Climate Change, edited by T. F. Stocker, D. Qin, G.-K.
413 Plattner, M. Tignor, S. K. Allen, J. Boschung, A. Nauels, Y. Xia, V. Bex and P. M. Midgley,
414 Cambridge University Press, Cambridge, United Kingdom and New York, NY, USA.

Myhre, G., et al. (2017a), Multi-model simulations of aerosol and ozone radiative forcing due to anthropogenic emission changes during the period 1990–2015, Atmos. Chem. Phys., 17(4), 2709-2720, doi: 10.5194/acp-17-2709-2017.

Myhre, G., et al. (2017b), PDRMIP: A Precipitation Driver and Response Model Intercomparison Project—Protocol and Preliminary Results, Bull. Am. Met. Soc., 98(6), 1185-1198, doi: 10.1175/bams-d-16-0019.1.

Otto, A., et al. (2013), Energy budget constraints on climate response, Nature Geoscience, 6(6), 415-416, doi: 10.1038/ngeo1836.

Poli, P., et al. (2016), ERA-20C: An Atmospheric Reanalysis of the Twentieth Century, J. Climate, 29(11), 4083-4097, doi: 10.1175/jcli-d-15-0556.1.

Proistosescu, C., and P. J. Huybers (2017), Slow climate mode reconciles historical and model-based estimates of climate sensitivity, Science Advances, 3(7), doi: 10.1126/sciadv.1602821.

Richardson, M., K. Cowtan, E. Hawkins, and M. B. Stolpe (2016), Reconciled climate response estimates from climate models and the energy budget of Earth, Nature Clim. Change, 6(10), 931-935, doi: 10.1038/nclimate3066.

Rose, B. E. J., and L. Rayborn (2016), The effects of ocean heat uptake on transient climate sensitivity, Current Climate Change Reports, 2(4), 190-201, doi: 10.1007/s40641-016-0048-4.

Rugenstein, M. A. A., K. Caldeira, and R. Knutti (2016), Dependence of global radiative feedbacks on evolving patterns of surface heat fluxes, Geophys. Res. Lett., 43(18), 9877-9885, doi: 10.1002/2016GL070907.

Santer, B. D., T. M. L. Wigley, J. S. Boyle, D. J. Gaffen, J. J. Hnilo, D. Nychka, D. E. Parker, and K. E. Taylor (2000), Statistical significance of trends and trend differences in layer-average atmospheric temperature time series, J. Geophys. Res., 105(D6), 7337-7356, doi: 10.1029/1999jd901105.

Sherwood, S. C., S. Bony, O. Boucher, C. Bretherton, P. M. Forster, J. M. Gregory, and B. Stevens (2014), Adjustments in the forcing-feedback framework for understanding climate change, Bull. Am. Met. Soc., 96(2), 217-228, doi: 10.1175/BAMS-D-13-00167.1.

Shindell, D. T. (2014), Inhomogeneous forcing and transient climate sensitivity, 4, 274, doi: 10.1038/nclimate2136.

445 Skeie, R. B., T. Berntsen, M. Aldrin, M. Holden, and G. Myhre (2014), A lower and more
446 constrained estimate of climate sensitivity using updated observations and detailed radiative
447 forcing time series, Earth System Dynamics, 5(1), 139-175, doi: 10.5194/esd-5-139-2014.
448 Stevens, B., S. C. Sherwood, S. Bony, and M. J. Webb (2016), Prospects for narrowing bounds
449 on Earth's equilibrium climate sensitivity, Earth's Future, 4(11), 512-522, doi:
450 10.1002/2016EF000376.
451 Stohl, A., et al. (2015), Evaluating the climate and air quality impacts of short-lived pollutants,
452 Atmos. Chem. Phys., 15(18), 10529-10566, doi: 10.5194/acp-15-10529-2015.
453 Stouffer, R. J., and S. Manabe (2017), Assessing temperature pattern projections made in 1989,
454 Nature Clim. Change, 7(3), 163-165, doi: 10.1038/nclimate3224.
455 Susskind, J., G. Molnar, L. Iredell, and N. G. Loeb (2012), Interannual variability of outgoing
456 longwave radiation as observed by AIRS and CERES, J. Geophys. Res., 117, doi:
457 10.1029/2012jd017997.
458 Taylor, K. E., R. J. Stouffer, and G. A. Meehl (2012), An overview of CMIP5 and the
459 experiment design, Bull. Am. Met. Soc., 93(4), 485-498, doi: 10.1175/bams-d-11-00094.1.
460 Tsushima, Y., and S. Manabe (2013), Assessment of radiative feedback in climate models using
461 satellite observations of annual flux variation, Proc. Natl. Acad. Sci., 110(19), 7568-7573,
462 doi: 10.1073/pnas.1216174110.
463 Tsushima, Y., A. Abe-Ouchi, and S. Manabe (2005), Radiative damping of annual variation in
464 global mean surface temperature: comparison between observed and simulated feedback,
465 Climate Dynamics, 24(6), 591-597, doi: 10.1007/s00382-005-0002-y.
466 Xie, S.-P., Y. Kosaka, and Y. M. Okumura (2016), Distinct energy budgets for anthropogenic
467 and natural changes during global warming hiatus, Nature Geoscience, 9(1), 29-33, doi:
468 10.1038/ngeo2581.
469 Xu, K. M., and K. A. Emanuel (1989), Is the tropical atmosphere conditionally unstable?, Mon.
470 Wea. Rev., 117(7), 1471-1479.
471 Zhou, C., M. D. Zelinka, and S. A. Klein (2016), Impact of decadal cloud variations on the
472 Earth/'s energy budget, Nature Geosci, 9(12), 871-874, doi: 10.1038/ngeo2828.
473

474

Acknowledgments: A.E.D. acknowledges support from NSF grant AGS-1661861 to Texas A&M University. P.M.F. acknowledges support from the Natural Environment Research Council project NE/P014844/1. We thank Bjorn Stevens and Thorsten Mauritsen for their insight into this analysis. We also acknowledge the modeling groups, the Program for Climate Model Diagnosis and Intercomparison, and the WCRP's Working Group on Coupled Modeling for their roles in making available the WCRP CMIP5 multimodel dataset. Radiative forcing can be found here: http://bit.ly/2FRE83c. All other data (CERES, CMIP5, reanalyses) are publicly available on the internet.

Table 1. Values for individual models

Model	λ_{iv}	Θ_{iv}	λ_{2xCO2}	Θ_{2xCO2}	$\Delta T_S/\Delta T_A$	$\Delta T_{S,tropics}/\Delta T_A$	$\Delta T_S/\Delta T_{S,tropics}$
ACCESS1-0	-0.69	-1.22	-0.75	-0.77	0.96	0.48	1.25
ACCESS1-3	-0.66	-0.86	-0.82	-0.74	0.91	0.46	1.19
BCC-CSM1-1	-0.74	-0.89	-1.21	-1.12	0.93	0.42	1.30
BCC-CSM1-1-M	-0.91	-0.94	-1.31	-1.23	0.92	0.51	1.15
CCSM4	-1.26	-1.25	-1.24	-1.26	0.99	0.58	1.26
CNRM-CM5	-1.14	-1.25	-1.11	-1.01	0.94	0.43	1.27
CNRM-CM5-2	-1.01	-1.25	-1.06	-0.94	0.89	0.41	1.21
CanESM2	-0.77	-0.73	-1.03	-0.90	0.88	0.49	1.16
FGOALS-g2	-1.55	-1.25	-0.83	-0.85	1.00	0.50	1.37
FGOALS-s2	-1.35	-1.60	-0.88	-0.77	0.87	0.47	1.20
GFDL-CM3	-0.21	-0.63	-0.75	-0.63	0.80	0.45	1.15
GFDL-ESM2G	-0.80	-1.24	-1.42	-0.98	0.68	0.43	1.02
GFDL-ESM2M	-1.41	-1.12	-1.34	-0.92	0.74	0.43	1.08
GISS-E2-H	-1.48	-0.36	-1.57	-1.36	0.91	0.26	1.35
GISS-E2-R	-1.03	-0.16	-1.70	-1.35	0.77	0.20	1.17
INMCM4	-0.65	-0.83	-1.51	-1.18	0.80	0.56	1.12
IPSL-CM5A-LR	-0.57	-0.61	-0.79	-0.54	0.71	0.49	1.04
IPSL-CM5A-MR	-0.46	-0.33	-0.81	-0.54	0.68	0.55	0.97
IPSL-CM5B-LR	-0.93	-0.94	-1.00	-0.87	0.91	0.45	1.33
MIROC5	-1.18	-0.90	-1.58	-1.13	0.84	0.57	1.18
MPI-ESM-LR	-0.78	-0.72	-1.14	-0.91	0.81	0.62	1.08
MPI-ESM-MR	-0.69	-0.76	-1.18	-0.93	0.80	0.52	1.05
MPI-ESM-P	-0.72	-0.70	-1.25	-0.98	0.80	0.58	1.09
MRI-CGCM3	-0.58	-1.29	-1.26	-1.11	0.88	0.40	1.21
NorESM1-M	-1.19	-1.13	-1.11	-1.15	1.02	0.47	1.34

Units on λ and Θ are $W/m^2/K$, other quantities are unitless. Methods of estimating these values are described in the methods section. $\Delta T_S/\Delta T_A$ and $\Delta T_S/\Delta T_{S,tropics}$ are calculated by differencing averages of the first and last decades of the abrupt $4xCO_2$ run. $\Delta T_{S,tropics}/\Delta T_A$ is estimated by regressing monthly values from the last 37 years of the abrupt $4xCO_2$ run.

Table 2. Values from the λ runs

run	mean	mode	median	5-95%	17-83%	%<2	%>4.5
all-Lambda-1	4.76	3.39	4.39	1.8-8.9	2.6-7.1	5	34
all-Lambda-2	3.79	2.31	3.30	1.4-8.0	2.0-5.7	15	26
good-Lambda-1	4.33	2.85	3.89	1.7-8.5	2.4-6.4	7	30
good-Lambda-2	3.66	2.31	3.19	1.4-7.7	1.9-5.4	17	24

Explanation of the run names is in the methods section.

Table 3. Values from the Θ runs

run	mean	mode	median	5-95%	17-83%	%<2	%>4.5
all-Theta-1	3.32	2.71	3.15	0.7-6.1	2.1-4.6	15	19
all-Theta-2	2.96	2.31	2.82	0.7-5.4	1.9-4.1	20	11
all-Theta-1-corr	3.36	2.58	3.14	0.8-6.4	2.0-4.8	16	20
noGISS-Theta-1	3.56	2.71	3.29	1.9-6.3	2.3-4.7	7	20
noGISS-Theta-2	3.18	2.31	2.95	1.7-5.5	2.1-4.2	13	13
good-Theta-1	3.54	2.58	3.31	2.0-5.9	2.4-4.7	5	20
good-Theta-2	3.43	3.12	3.32	1.9-5.4	2.4-4.4	6	15
good-Theta-1-corr	3.55	2.44	3.29	1.9-6.1	2.3-4.8	6	21
good-Theta-1-normal	3.54	3.12	3.39	1.8-5.8	2.4-4.6	8	19

Explanation of the run names is in the methods section.

Table 4. Error budget calculations

run	mean	mode	median	5-95%	17-83%	%<2	%>4.5
error-goodTheta-2-noF	3.43	3.25	3.33	1.9-5.3	2.4-4.4	6	15
error-goodTheta-2-noRat	3.43	3.25	3.36	2.4-4.7	2.8-4.0	0	7
error-goodTheta-2-nodtdt	3.43	3.25	3.35	2.0-5.2	2.4-4.4	5	14
error-goodTheta-2-noTheta	3.34	3.53	3.35	2.1-4.9	2.4-4.2	4	10

Explanation of the run names is in the methods section.

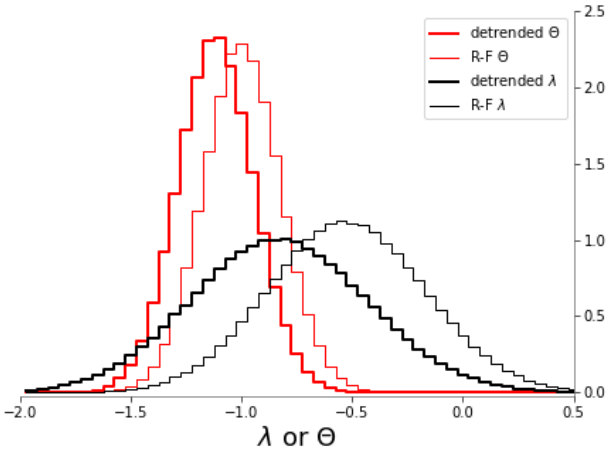

Figure 1. Distribution of λ_{iv} and Θ_{iv} from observations. Distributions calculated using detrended and R-F regressions are both shown.

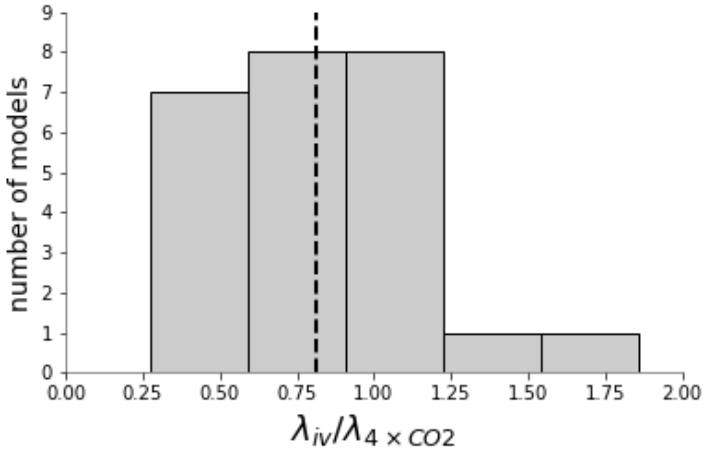

Figure 2. Distribution of $\lambda_{iv}/\lambda_{4xCO2}$ from 25 CMIP5 models; the black dashed line is the mean of the distribution. See methods for description of how the value is calculated in each model.

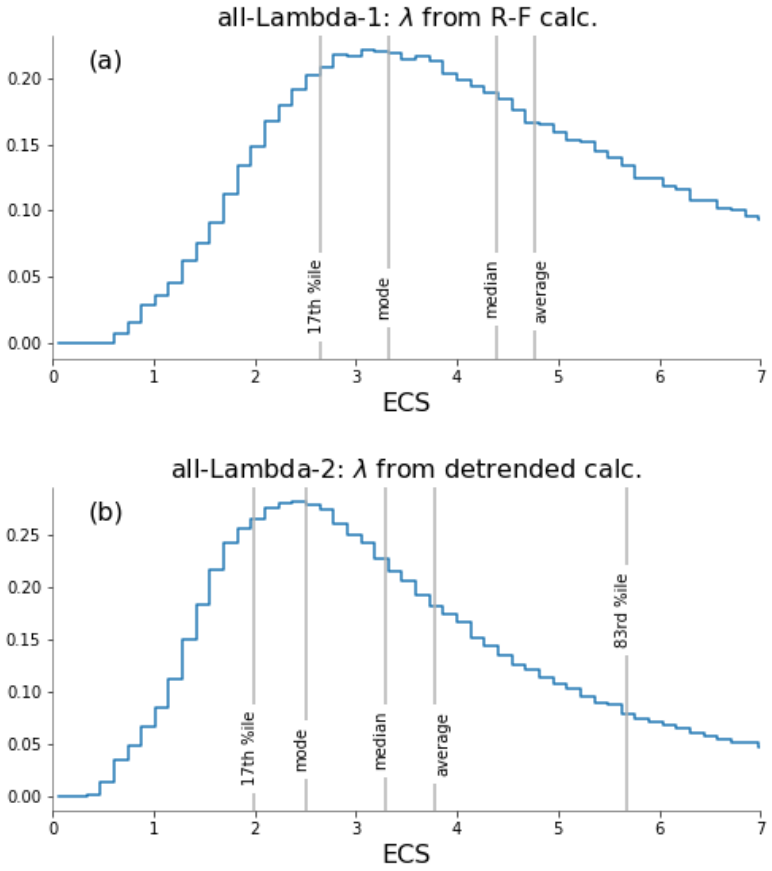

Figure 3. Distributions of ECS using the traditional energy balance framework (Eq. 4). (a) Distribution using λ_{iv} from the R-F regression, (b) Distribution using λ_{iv} from the detrended regression. "17th %ile" and "83rd %ile" are 17th and 83rd percentile, corresponding to the IPCC's *likely* range.

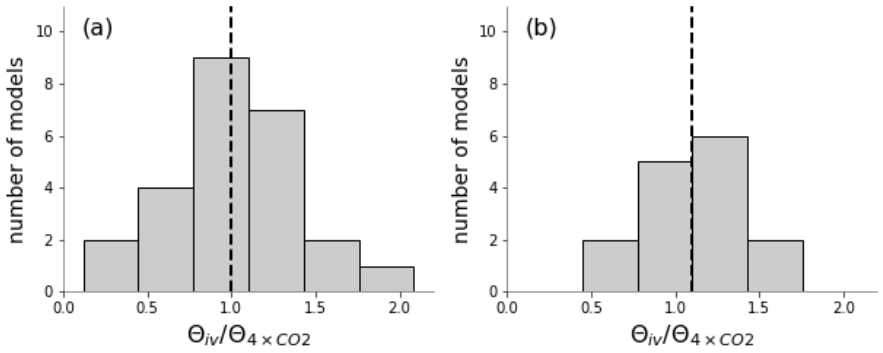

Figure 4. Distribution of $\Theta_{iv}/\Theta_{4xCO2}$ from (a) 25 CMIP5 models and (b) from those 15 models whose Θ_{iv} agrees with observations. The black dashed lines are the means of the distributions. See methods for description of how this is calculated in each model.

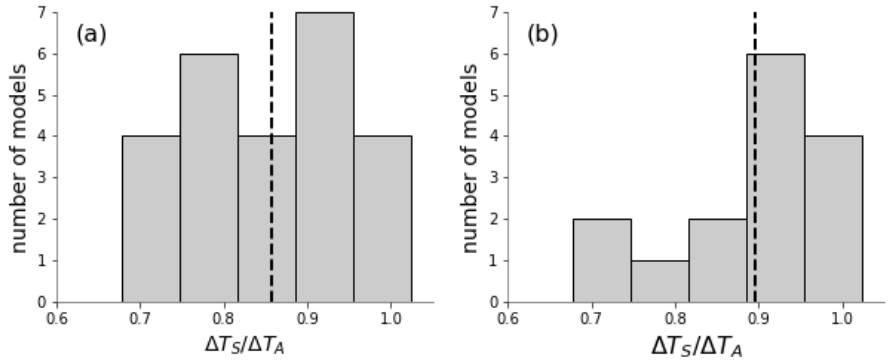

Figure 5. Distribution of $\Delta T_S/\Delta T_A$ from (a) 25 CMIP5 models and (b) from those 15 models whose Θ_{iv} agrees with observations. Calculated by differencing the average of the first and last decades of the CMIP5 ensemble's abrupt $4xCO_2$ runs. The black dashed lines are the means of the distributions.

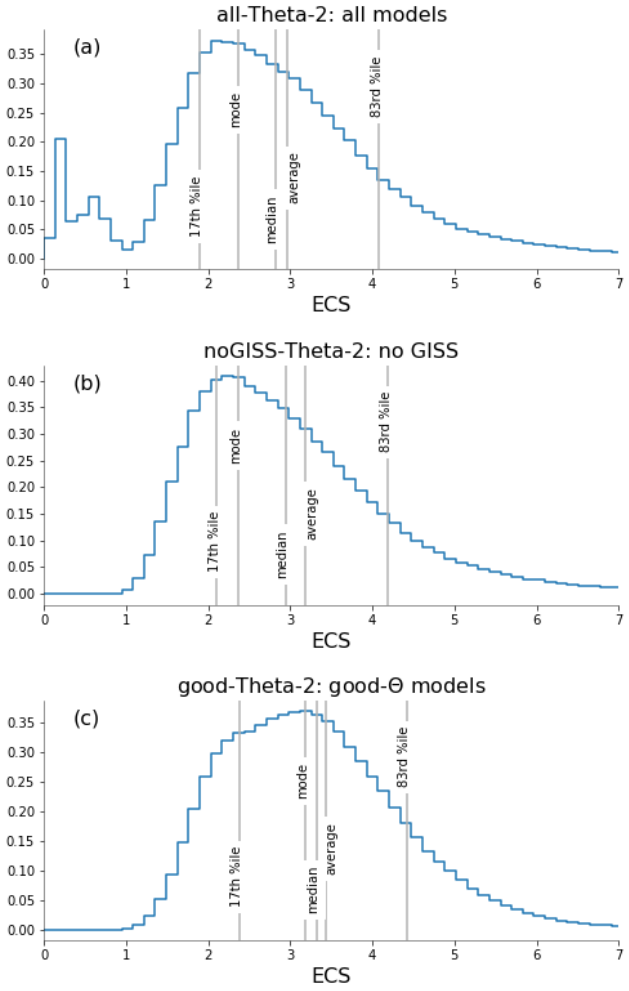

Figure 6. Distributions of ECS using the revised energy balance framework (Eq. 6) (a) using all models, (b) using all models except for the two GISS models, (c) using 15 models whose Θ_{iv} agrees with the value estimated from observations. All calculations use Θ_{iv} from the detrended calculation; using Θ_{iv} from the R-F calculation produces nearly identical results. "17th %ile" and "83rd %ile" are 17th and 83rd percentile, corresponding to the IPCC's *likely* range.

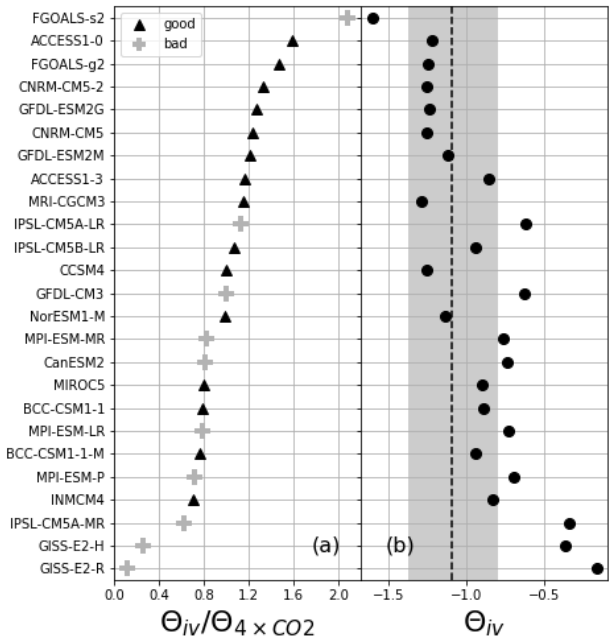

Figure 7. CMIP5 model estimates of (a) $\Theta_{iv}/\Theta_{2xCO2}$ and (b) Θ_{iv}. The gray region in panel b shows the observational range (from the CERES detrended calculation). The black triangle symbols in panel a) indicate that the model's Θ_{iv} agrees with observations; the gray cross symbols indicate that it does not.

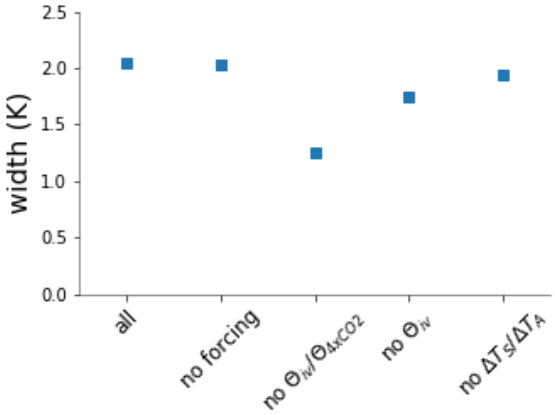

Figure 8. Error budget analysis of ECS estimates. The "all" data are the widths of the full ECS distribution from the good-Theta-2 calculation (Table 3). Then, from left to right, is the width when the uncertainty in forcing, $\Theta_{iv}/\Theta_{4xCO2}$, Θ_{iv}, and $\Delta T_S/\Delta T_A$ distributions are sequentially set to zero. Dots show uncertainty as measured by the difference between the 17th and 83rd percentile of the ECS distribution.

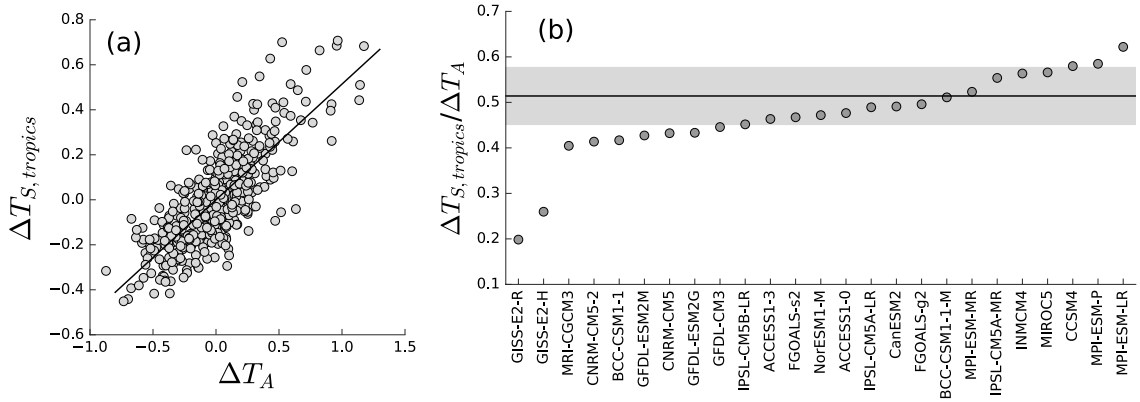

Figure 9. Estimates of $\Delta T_{S,tropics}/\Delta T_A$. (a) Scatter plot of monthly $\Delta T_{S,tropics}$ (tropical avg. surface temperature) anomalies vs. ΔT_A anomalies from ERAi reanalysis. The solid line is the best fit line. (b) The slope of the fit to the same regression from the last 37 years of the CMIP5 ensemble's abrupt $4xCO_2$ runs. The black line and gray region shows the slope and uncertainty of the fit to observations in panel a.

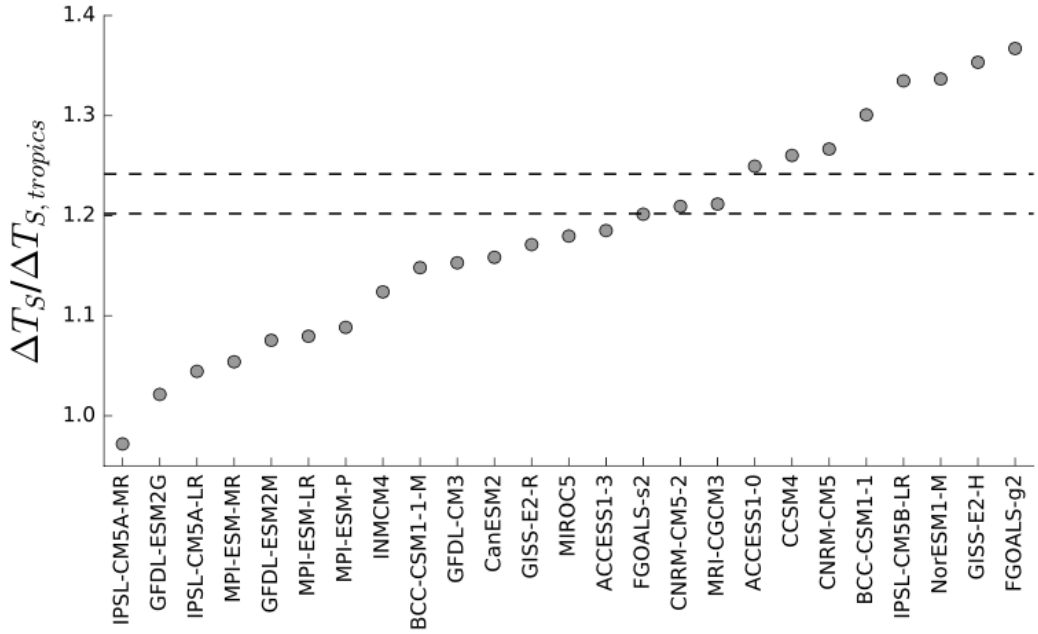

Figure 10. Estimates of polar amplification in the models, $\Delta T_S/\Delta T_{S,tropics}$. For the CMIP5 ensemble, this is calculated by differencing the average of the first and last decades of the CMIP5 ensemble's abrupt $4xCO_2$ runs. The two dashed lines are observational estimates (see text).